JOURNAL OF ENVIRONMENTAL SCIENCES 137 (2024) 626–638

Available online at www.sciencedirect.com

ScienceDirect

www.elsevier.com/locate/jes

JES JOURNAL OF ENVIRONMENTAL SCIENCES

www.jesc.ac.cn

Research Article

Efficient reduction and adsorption of Cr(VI) using $FeCl_3$-modified biochar: Synergistic roles of persistent free radicals and Fe(II)

Shujie Hu[1,4], *Chengshuai Liu*[1,2,*], *Hongling Bu*[1,5], *Manjia Chen*[1], *Ying-heng Fei*[3,*]

[1] *National-Regional Joint Engineering Research Center for Soil Pollution Control and Remediation in South China, Guangdong Key Laboratory of Integrated Agro-environmental Pollution Control and Management, Institute of Eco-environmental and Soil Sciences, Guangdong Academy of Sciences, Guangzhou 510650, China*

[2] *State Key Laboratory of Environmental Geochemistry, Institute of Geochemistry, Chinese Academy of Science, Guiyang 550081, China*

[3] *School of Environment Science and Engineering, Guangzhou University, Guangzhou 510006, China*

[4] *College of Resources and Environment, Chongqing School, University of Chinese Academy of Sciences, Chongqing 400714, China*

[5] *School of Environmental Science and Engineering, Guangdong University of Technology, Guangzhou 510006, China*

ARTICLE INFO

Article history:
Received 14 December 2022
Revised 7 March 2023
Accepted 7 March 2023
Available online 21 March 2023

Keywords:
Biochar
Iron-modification
Cr(VI)
Electron transfer
Reduction mechanism

ABSTRACT

Transition metal iron and persistent free radicals (PFRs) both affect the redox properties of biochar, but the electron transfer relationship between them and the coupling reduction mechanism of Cr(VI) requires further investigation. To untangle the interplay between iron and PFRs in biochar and the influences on redox properties, $FeCl_3$-modified rice husk biochar (FBCs) was prepared and its reduction mechanism for Cr(VI) without light was evaluated. The FBCs had higher surface positive charges, oxygen-containing functional groups, and PFRs compared with pristine rice husk biochar (BC). Phenoxyl PFRs with high electron-donating capability formed in biochar. The pronounced electron paramagnetic resonance signals showed that the PFRs preferred to form at lower Fe(III) concentrations. While a high concentration of Fe(III) would be reduced to Fe(II) and consumed the formed PFRs. Adsorption kinetics and X-ray photoelectron spectroscopy analysis indicated that the FBCs effectively enhanced the Cr(VI) removal efficiency by 1.54-8.20 fold and the Cr(VI) reduction efficiency by 1.88-9.29 fold compared to those of BC. PFRs quenching and competitive reductant addition experiments revealed that the higher Cr(VI) reduction performance of FBCs was mainly attributed to the formed PFRs, which could contribute to ~74.0% of Cr(VI) reduction by direct or indirect electron transfer. The PFRs on FBCs surfaces could promote the

* Corresponding authors.
E-mails: liuchengshuai@vip.gyig.ac.cn (C. Liu), yhfei@gzhu.edu.cn (Y.-h. Fei).

https://doi.org/10.1016/j.jes.2023.03.011

Fe(III)/Fe(II) cycle through single electron transfer and synergistically accelerate ~52.3% of Cr(VI) reduction. This study provides an improved understanding of the reduction mechanism of iron-modified biochar PFRs on Cr(VI) in environments.

Introduction

Biochar, derived from incomplete biomass combustion, is a carbon-rich substance with abundant surface functional groups and developed micropore structures (Mandal et al., 2021; Vithanage et al., 2017). Recently, biochar has received extensive attention due to its application in improving soil fertility, sequestering carbon, and controlling the migration of contaminants (Lehmann et al., 2011). Many investigators have shown the excellent adsorption ability of organic contaminants and toxic metal ions on biochar (Hu et al., 2019; Zhao et al., 2018). A few of the findings regarding the redox properties of biochar have been documented (Cuong et al., 2021; Shen et al., 2021). For example, biochar can accept or donate several hundred micromoles of electrons per gram due to its abundant phenolic, and quinone moieties, as well as conjugated π-electrons (Kemper et al., 2008; Klüpfel et al., 2014; Xu et al., 2013).

Persistent free radicals (PFRs), generated from pyrolysis or hydrothermal carbonization of biomass, have been found on biochar surfaces and can affect the redox properties of biochar (Chacón et al., 2020; Zhu et al., 2020; Zhao et al., 2018; Fang et al., 2015). In addition, the significant effect of PFRs type on the redox properties of biochar has been reported (Chen et al., 2021; Ruan et al., 2019; Zhong et al., 2018). For instance, carbon-centered PFRs (i.e., cyclopentadiene radicals) have a strong electron-supplying capacity (Zhong et al., 2018). Oxygen-centered PFRs (i.e., semiquinone radicals) can be invoked as temporary electron carriers to participate reversibly in redox reactions (Xu et al., 2019). Recently, transition metals have been discovered as one key factor determining the formation and stability of biochar PFRs (Ruan et al., 2019; Fang et al., 2015). Exogenous Fe(III) could facilitate the decarboxylation of organic matter during biochar pyrolysis and promote the formation of PFRs (Vejerano et al., 2011). However, Fang et al. (2015) found that the excess exogenous Fe(III) would consume the formed PFRs, since PFRs can act as an electron donor to mediate the reduction of Fe(III) to Fe(II). Therefore, transition metal ions may exhibit a double-effect in the formation of PFRs, yet this double-effect on biochar redox properties needs to be further verified.

Chromium (Cr), a redox-active metal element, predominately exists in two states, namely Cr(III) and Cr(VI) (Xu et a., 2020b; Park et al., 2004). Cr(VI) in the form of an oxyanion (i.e., CrO_4^{2-}) is regarded as a typical toxic contaminant by the U.S. EPA due to its impacts on chronic liver damage and pulmonary congestion (Zhu et al., 2020; Gonzalez et al., 2005). The toxic risks are mainly from the high mobility of Cr(VI) owing to repulsive electrostatic interactions between the Cr(VI) oxyanion and negatively charged soil or sediment (Fendorf, 1995). Cr(III) is of low toxicity and mobility compared with Cr(VI) and plays an important role in sugar and fat metabolism as essential for living organisms (Pechova and Pavlata, 2007). Therefore, the transformation of Cr(VI) to Cr(III) is an important process of soil Cr(VI) remediation. Recently, PFRs on biochar could trigger a successive single-electron transfer reaction to Cr(VI) detoxification has been demonstrated (Zhu et al., 2020; Yang et al., 2016a). However, biochar has a relatively weak adsorption affinity for Cr(VI) due to its negative surface charge, further restricting its conversion of Cr(VI) to Cr(III) (Wang et al., 2020). Iron modification can regulate the surface charge and produce reductive Fe(II) or Fe^0 on biochar, and the porous structure of biochar can reduce the agglomerations of these highly activated Fe, thus improve the adsorption-reduction ability of Cr(VI) (Liu et al., 2020; Su et al., 2021; Wang et al., 2020; Zhong et al., 2018; Zhou et al., 2022). Additionally, due to the magnetic effect of iron, iron-modified biochar can be easily separated and has been widely used in soil remediation (Zhong et al., 2018). However, they did not focus on the coupling electron transfer mechanism of iron and PFRs on iron-modified biochar for Cr(VI) reduction. Additionally, enhanced electron transfer of biochar PFRs by ultraviolet or visible-light irradiation has been documented (Chen et al., 2021; Tang et al., 2021; Yi et al., 2021). These photo-derived PFRs, different from that derived during pyrolysis processes, are reversible and unstable, which was documented to induce the release of electrons to oxygen and promote the generation of active free radicals, thus improved the degradation or transformation of pollutants (Shi et al., 2020; Tang et al., 2021). Whilst, the studies on the transformation of heavy metals without light (such as soil environment) and the contribution mediated by the pyrolysis irradiated PFRs in the iron-modified biochar are limited.

For this purpose, iron-modified biochar was prepared by infiltrating rice husk with $FeCl_3$ before slow pyrolysis and its reduction mechanism for Cr(VI) without light was evaluated. The objectives of this work were (1) to study the surface properties (functional groups, electronic charge, etc.) and PFRs of biochar after $FeCl_3$ modification, and (2) to investigate the removal performance and reduction mechanism of Cr(VI) for $FeCl_3$-modified biochar, as well as (3) to clarify the coupling electron transfer mechanism and contribution of $FeCl_3$-modified biochar from PFRs and Fe(II) to Cr(VI) in the natural dark environment.

1. Materials and methods

1.1. *Preparation of biochar and iron-modified biochar*

Rice husk, a typical agricultural waste, was chosen as biomass. The collected rice husk was washed with distilled water, dried at 60°C for 24 hr, and crushed to pass through a 60-mesh sieve. The biochar was produced by slow pyrolysis under an oxygen-limited condition as previously reported

(Zhang et al., 2019). Briefly, crushed biomass was pyrolyzed under the N_2-atmosphere with a temperature programming process as follows: 100°C for 30 min, and then elevated to 300°C (400, 500, 600, 700, and 800°C) at 10 °C/min and maintained for 2 hr. The PFRs concentration of biochar at different temperatures was measured using electron paramagnetic resonance (EPR). The highest PFRs concentration was found at 500°C (Appendix A **Fig. S1a**). Therefore, the subsequent iron-modified biochar samples (FBCs) were pyrolyzed at 500°C, and the pristine biochar pyrolyzed at 500°C was named BC.

Rice husk powders were impregnated in $FeCl_3$ solution for 12 hr at Fe/biomass of 1% and 5% (W/W). Then the mixture was dried at 80°C and ground before thermal treatment. The powdered samples were slowly pyrolyzed at 500°C under a N_2 atmosphere for 2 hr, yielding FBC-1 and FBC-5, respectively.

1.2. *Characterization of biochar and iron-modified biochar*

The C, H, and N contents of the samples were measured using a Vario EL CUBE elemental analyzer (Elementar, Germany), and the O contents were analyzed with a Vario ELIII elemental analyzer (Elementar, Germany). The CO_2 isotherms were measured at 273 K using a Micromeritics ASAP 2020 surface area and pore size analyzer at a relatively atmospheric pressure of 1×10^{-6} to 0.03 (Micromeritics, America). The surface charges of the biochar samples at different pH values (3-11) were measured in terms of zeta potential by a Malven MPT-2/Zeta sizer Nano ZS instrument (Mastersizer 3000, Britain). The solid surface chemistry and microscopic features of biochar and iron-modified biochar were characterized by scanning electron microscopy (SEM, TESCAN MIRA4, Britain) with an energy-dispersive spectrometer (EDS, Oxford, Britain). The crystal iron minerals in the biochar were characterized by X-ray diffraction (XRD); data were collected from 10° to 80° 2θ with a step size of 0.02 degrees and 1.0 sec per step using Co Kα radiation (D2 Phaser, Bruker, Germany). The oxygen functional groups of the biochar samples were evaluated by Fourier transform infrared spectrometer (FTIR, IRTrace-100, Shimadzu, Japan) in the region of 400–4000 cm^{-1} with a resolution of 4 cm^{-1}. The surface elemental composition (C, N O, Fe, and Cr) and carbon-based functional groups of the biochar samples were measured by X-ray photoelectron spectroscopy (XPS) with a K-Alpha instrument (Thermo Scientific, Britain).

1.3. *EPR measurements and PFRs quenching experiments*

Biochar solid samples. A total of 20 mg of BC or FBCs was injected into a micropipette in an EPR instrument (Bruker A300 spectrometer, Germany) under ambient conditions. The specific parameters were as follows: center field 3510 G, sweep width 300 G, microwave frequency 9.85 GHz, microwave power 19.23 mW, modulation frequency 100 kHz, modulation amplitude 1.0 G, and sweep time 60.42 sec (Liang et al., 2020; Zhu et al., 2020).

$O_2^{\bullet-}$ measurement in solutions. The $O_2^{\bullet-}$ was characterized by EPR coupled with 5,5-dimethyl-l-pyrroline-N-oxide (DMPO) as a spin-trapping agent (Han et al., 2022). Briefly, each 5.0 g/L biochar suspension was filtered after 10 min of shock in the dark. The filtered solution was then mixed with 100 mmol/L trapping agents at a 1:1 volume ratio to obtain 1.0 mL of the mixed solution. Then, 30 μL of the mixed solution was absorbed into a capillary glass tube for the EPR test.

PFRs quenching experiments. To probe the role of PFRs in FBCs and identify their impacts on Cr(VI) reduction or Cr(III) generation, 200 mmol/L methanol (MeOH) was used as an electron competitor during the quenching tests (Zhu et al., 2020). Moreover, pre-extraction was conducted before the kinetic tests by adding 10 mL MeOH to 1.0 g FBCs three times to completely quench PFRs (Zhu et al., 2020).

1.4. *Batch sorption kinetic and isotherm sorption experiments*

The sorption kinetic experiment was performed by adding 1.0 g of biochar samples to 200 mL 100 mg/L Cr(VI) solution in a 250 mL glass bottle. The pH was adjusted to 5.0 ± 0.1 by adding 0.1 mol/L HCl or NaOH solution. No buffer was added in these experiments. All sorption experiments were repeated three times. The kinetic experiments were carried out under dark conditions at 25 ± 1°C and 500 r/min. The samples were removed from the solution at different reaction times (0, 0.17, 0.5, 1, 2, 4, 8, 12, 24, and 48 hr), followed by filtering through a 0.45-μm membrane. Then, biochar particles were collected at 48 hr, rinsed with deionized water, and freeze-dried before XPS and EPR analyses. The Cr(VI) concentration was determined by the 1,5-diphenylcarbazide (DPC) colorimetric method at 540 nm using a UV-visible near-infrared spectrophotometer (UV-3600plus, Shimadzu, Japan) (Zhu et al., 2020). Total Cr was measured by inductively coupled plasma optical emission spectrometry (ICP-OES) (Optima 8000, PerkinElmer, Singapore). The generated Cr(III) concentrations were approximated by subtracting the Cr(VI) concentration from the total Cr in the aquatic phase (Zhu et al., 2020; Zhong et al., 2018). The concentrations of total Fe and Fe(II) were identified using the 1,10-phenanthroline method (Tamura et al., 1974). Sorption kinetic models of pseudo-first-order (PFO), pseudo-second-order (PSO), and Elovich were detailed in Supplementary materials.

For isotherm sorption experiments, the Cr(VI) concentration was in the range of 5 to 1000 mg/L. The Cr(VI) solution and biochar were mixed at a ratio of 200:1 in 15 mL centrifuge tubes. The centrifuge tubes were shaken under the dark condition at 25 ± 1°C and 500 r/min for 48 hr. Then, the concentrations of Cr(VI), total Cr, total Fe, and Fe(II) in the solution were determined. Sorption isotherm models of Freundlich and Langmuir were listed in Supplementary materials.

2. Results and discussion

2.1. *Cr(VI) removal and reduction performance*

The predominant form of Cr(VI) in the solution was $HCrO_4^-$, which exists in the pH range of 1.0-6.3 (Rajput et al., 2016). BC had a low efficiency in removing Cr(VI) from aqueous solution, with Cr(VI) decreasing from 100 to 89.2 mg/L within 48 hr (Fig. 1a). The aqueous Cr(III) concentration of the BC system first increased to 5.80 mg/L (0-0.17 hr) and then gradually decreased to 3.48 mg/L (0.17-48 hr). The electrostatic attraction

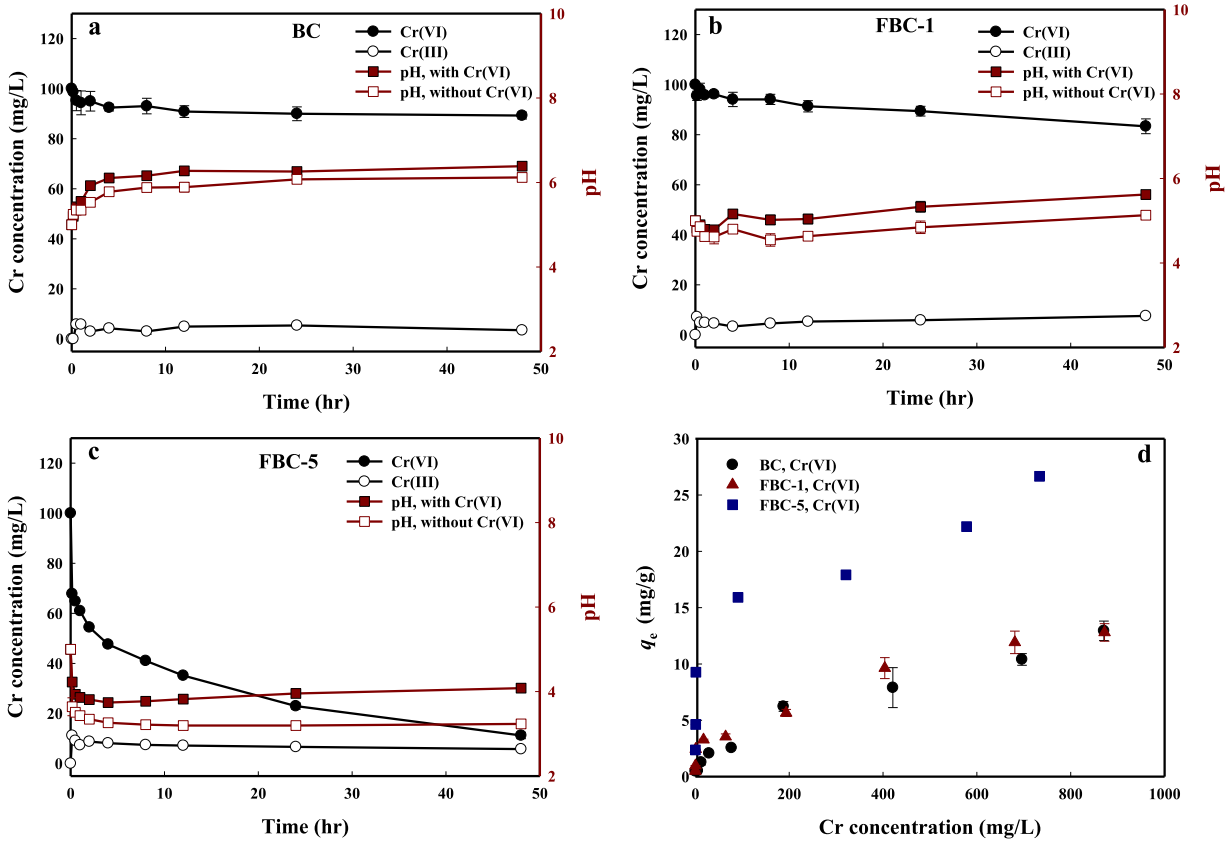

Fig. 1 – Cr(VI) removal kinetics (black solid) and Cr(III) formation kinetics (black hollow) of BC (a), FBC-1 (b), and FBC-5 (c). Cr(VI) adsorption isotherms of BC and FBCs (d). In figures a-c, red solid squares represent pH changes in experimental group (with Cr(VI)). The red hollow squares represent pH changes in control group (without Cr(VI)). Conditions of figures a-c: [Biochar] = 5.0 g/L, [initial Cr(VI)] = 100 mg/L, [initial pH] = 5.0 ± 0.1, [temperature] = 25 ± 1°C.

between the negative surface charge of BC and Cr(III) may decrease the Cr(III) concentration (solution pH=5.2–6.39, Fig. 1a and Appendix A Fig. S1b). In addition, the solution pH eventually increased to 6.39 due to the alkalinity of BC (pH=11.1, Appendix A Table S1). At higher pH in the solution, the generated Cr(III) tends to precipitate on the BC surface, resulting in high passivation of BC, which limits the further reaction of Cr(III) or Cr(VI) (Fei et al., 2022; Dong et al., 2017; Liang et al., 2014). The Cr(VI) concentrations of FBC-1 and FBC-5 systems decreased from 100 to 83.4 and 100 to 11.2 mg/L within 48 hr (Fig. 1b and 1c), respectively. FBCs showed higher Cr(VI) removal efficiencies of 16.6% and 88.8% than that BC (10.8%) did. FBCs, especially FBC-5, had more positive surface charge than BC (Appendix A Fig. S1b), indicating a stronger electrostatic attraction with Cr(VI). This may be the cause of the rapid removal of Cr(VI) in the initial stage. In addition, FBC-5 exhibited more honeycomb and tunnel structures than BC, suggesting more active sites for adsorbing Cr(VI) (Appendix A Fig. S2). The aqueous Cr(III) concentrations of FBC-1 and FBC-5 systems were 7.20 and 11.2 mg/L at 0.17 hr, respectively, higher than that of BC (5.80 mg/L), indicating higher reduction abilities of FBCs than BC. Moreover, the final pH values of BC, FBC-1, and FBC-5 were 6.39, 5.62, and 4.08, respectively, which were greater than those in the control groups without Cr(VI) (6.12, 5.13, and 3.24, respectively), illustrating that the reduction of Cr(VI) consumed protons (Fig. 1a-c). The above results showed that Cr(VI) removal by BC and the FBCs was a hybrid adsorption and reduction process.

Three kinetic models, PFO, PSO, and Elovich were presented in Appendix A Table S2. The PFO and PSO models for BC and FBCs did not fit the Cr(VI) removal data well, with R^2 values ranging from 0.489 to 0.963, indicating that the adsorption sites on the surface of BC and FBCs were not the sole factor that controls the Cr(VI) removal (Kyzas et al., 2012; Lima et al., 2018). Especially for FBC-5, the R^2 values of the PFO and PSO models were poor at 0.489 and 0.700, respectively. The Elovich model reproduced the experimental data with higher coefficient values ($R^2 \geq 0.933$), suggesting that the adsorption of Cr(VI) is a chemical process on a heterogeneous surface (Wu et al., 2009). The smaller the β value in Elovich's model is, the stronger the chemical action is (Lima et al., 2018). FBC-5 had the lowest β value of 0.47 g/mg, revealing a strong chemical interaction between active groups on its surface with the Cr(VI).

Fig. 1d showed the sorption isotherms of Cr(VI) for BC and FBCs. The sorption capacity q_m of FBC-5 for Cr(VI) was the largest (24.3 mg/g), consistent with the kinetic results. The better R^2 values of 0.863-0.988 fitted by the Freundlich model than the Langmuir model (0.816-0.979) (Appendix A Table S3) suggested that the sorption of Cr(VI) on biochar sam-

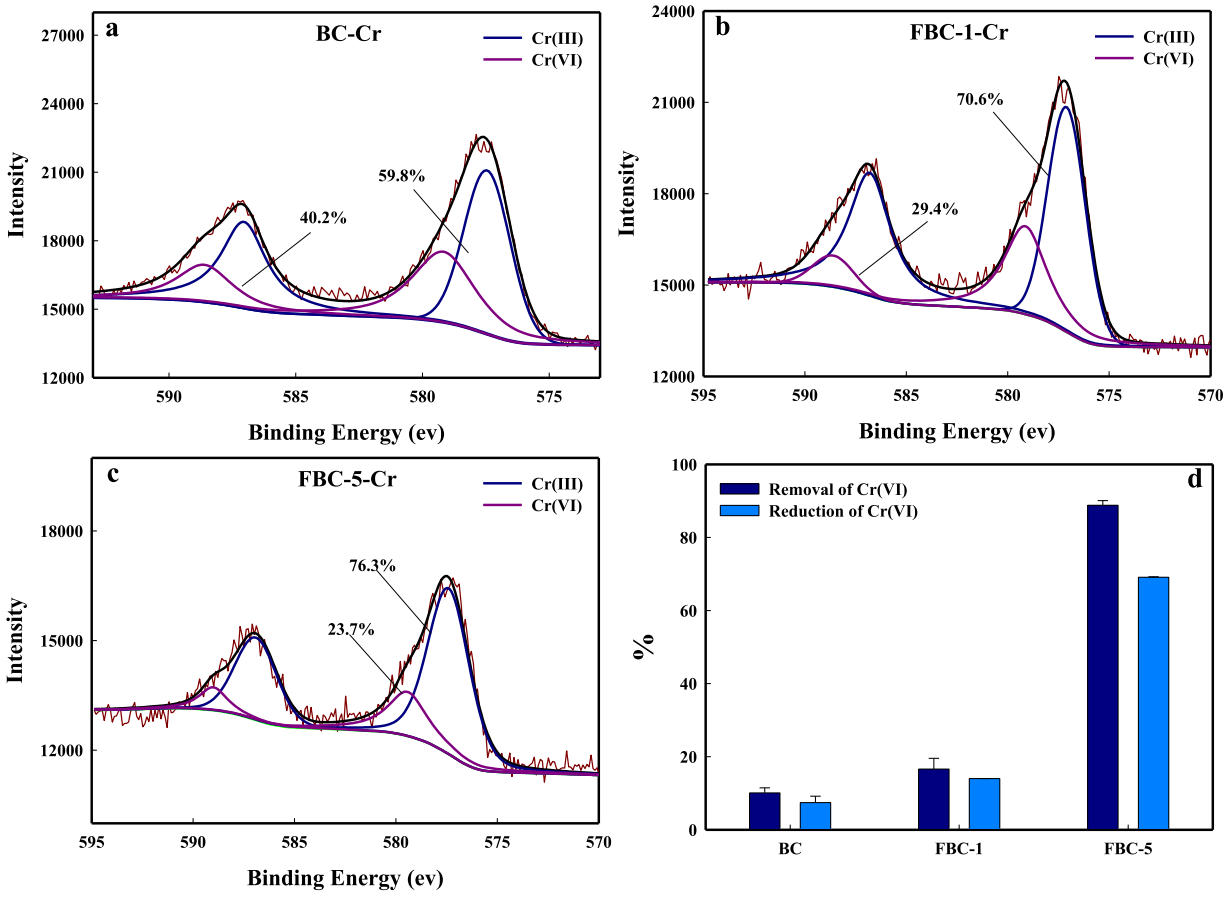

Fig. 2 – Cr 2p3/2 XPS spectra of BC (a), FBC-1 (b), and FBC-5 (c) after Cr(VI) removal. Cr(VI) removal and reduction efficiency (d) of BC and FBCs.

ples was a heterogeneous process (i.e., multilayered adsorption) rather than a homogeneous process (i.e., monolayer coverage) (Su et al., 2021; Zhu et al., 2020). This also explained that although the micropore volume of FBC-5 was smaller than that of FBC-1 (Appendix A Fig. S1c and Table S1), the removal efficiency of Cr(VI) was higher than that of FBC-1. The above kinetic and isotherm analysis indicated that the removal of Cr(VI) by BC and FBCs was a complex chemisorption process.

XPS analyses were used to identify the Cr(VI) reduction by BC and FBCs. A Cr peak was found in the XPS survey scan, indicating Cr adsorption/precipitation on the BC and FBCs surface (Appendix A Fig. S3). 59.8% of Cr sorbed in BC was Cr(III) (576.9 and 586.8 eV), and the remaining 40.2% was Cr(VI) (579.8 and 589 eV) (Fig. 2a). In contrast, the sorbed Cr(III) on the FBC-1 and FBC-5 surfaces increased to 70.6% and 76.3%, respectively (Fig. 2b and 2c). In addition, reduction efficiency of Cr(VI) was evaluated by adding the Cr(III) that adsorbed on the biochar surface and generated in the aqueous solution. The reduction efficiencies of Cr(VI) by BC, FBC-1, and FBC-5 were 7.44%, 14.0%, and 69.1%, accounting for 73.7%, 84.3%, and 77.8% of the removal efficiency of Cr(VI), respectively (Fig. 2d). The above results revealed that $FeCl_3$-doping enhanced the reduction efficiency of Cr(VI) by biochar. The reduction was the main removal mechanism of Cr(VI) by BC and FBCs.

2.2. *Functional organic groups involved in Cr(VI) reduction*

The O-containing functional groups on the biochar surface may adsorb or reduce Cr(VI) by complexation or redox processes (Fei et al., 2022; Zhang et al., 2020). Substantial changes were observed in the XPS spectra of C1s and O1s on BC and FBCs before and after Cr(VI) removal (Fig. 3). In O1s spectra, peaks at 531.3 and 533.5 eV are surface-adsorbed oxygen (O_A) and molecular oxygen (O_S), respectively (Mian et al., 2018; Yang et al., 2016b). The contents of O_A and total O for BC and FBCs after Cr(VI) removal increased from 1.78%-7.71% to 7.20%-10.8% and from 18.1%-24.0% to 20.5%-28.6% (Appendix A Table S4), respectively, possibly due to that chromium oxides were formed on the BC and FBCs surface (Mian et al., 2018; Yang et al., 2016b). About 13.6% and 3.96% of the C atoms on BC were surface reductive C-O (286.5 eV) and surface oxidative C=O groups (288.5 eV), respectively (Liu et al., 2020) (Appendix A Table S4). The C-O groups on the FBC-1 and FBC-5 significantly increased to 29.2% and 28.6%, respectively, consistent with a previous study (Liu et al., 2020), while C=O groups (3.30% and 4.25%, respectively) on the FBC-1 and FBC-5 surface showed little changes compared with that on BC, indicating that $FeCl_3$ mainly increased the surface reductive groups of biochar. After Cr(VI) removal, the reductive C-O groups on BC

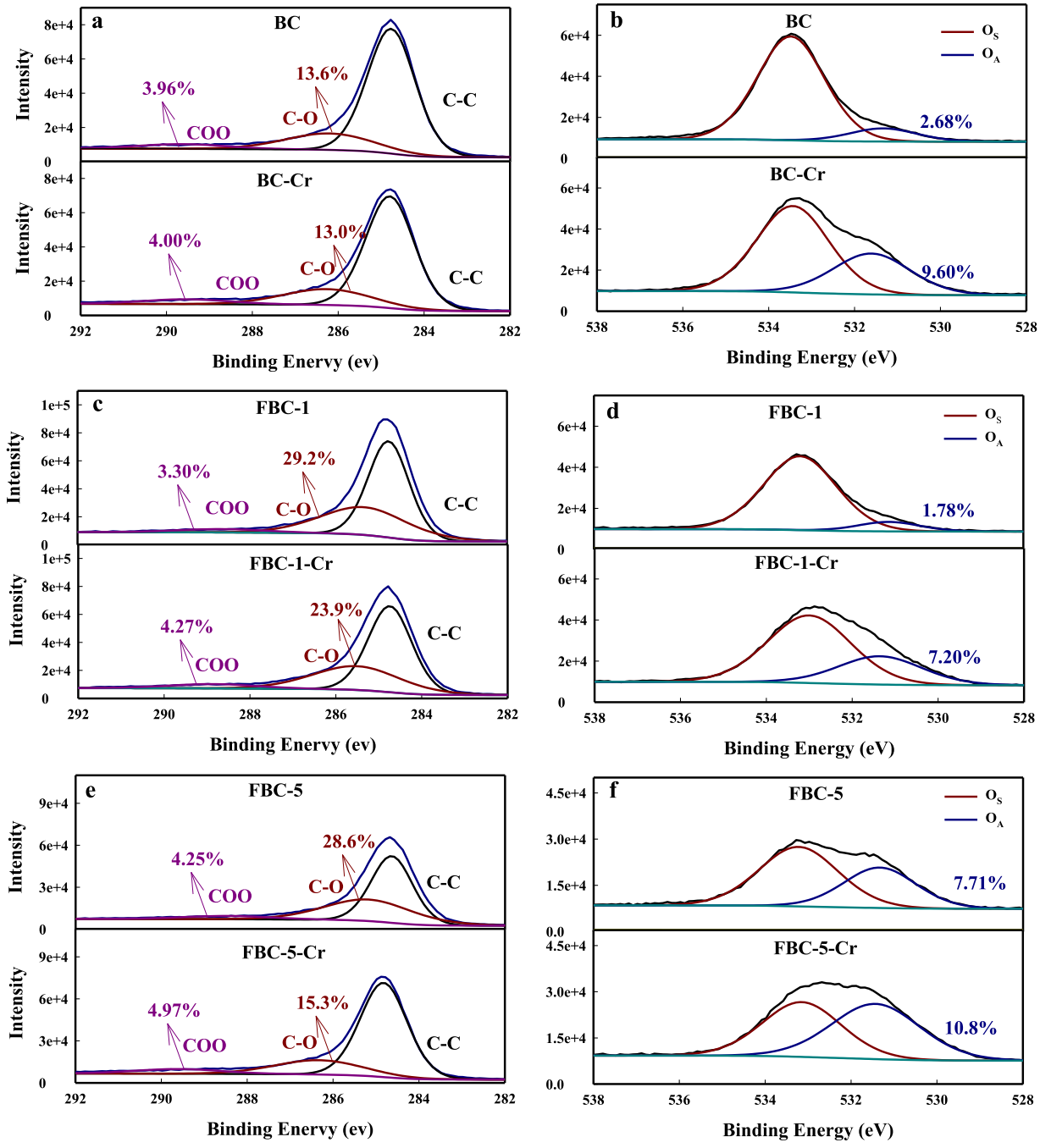

Fig. 3 – C1s and O1s XPS spectra of BC and FBCs before and after Cr(VI) removal. In figures b, d, and f, O_S represents molecular oxygen and O_A represents surface-adsorbed oxygen.

decreased slightly from 13.6% to 13.0%, and on the FBCs, these groups decreased conspicuously from 28.6%-29.2% to 15.3%-23.9% (Fig. 3 and Appendix A Table S4). In contrast, a slight increase in C=O groups from 3.30%-4.25% to 4.00%-4.97% was observed on the surfaces of the BC and FBCs after Cr(VI) removal, which is theoretically expected and is consistent with empirical observations by others that phenolics were oxidized to carboxylic groups (Liu et al., 2020; Zhang et al., 2020). In addition, the decreased intensity of phenolic-OH groups and the increased intensity of carboxyl -COO groups were also observed in the FTIR spectra of BC and FBCs after Cr(VI) removal (Appendix A Fig. S4). However, the decreased contents in C-O of BC and FBCs were much higher than the increased contents in C=O, suggesting that C-O may mainly adsorb Cr(VI) through complexation, while its reduction effect on Cr(VI) is limited. Moreover, it was reported that biochar could release dissolved organic matter (DOM) after entering water environment, which may transfer electron to reduce the Cr(VI) into Cr(III) (Dong et al., 2014; Chen et al., 2021). However, the removal efficiency of Cr(VI) by BC-derived DOM in

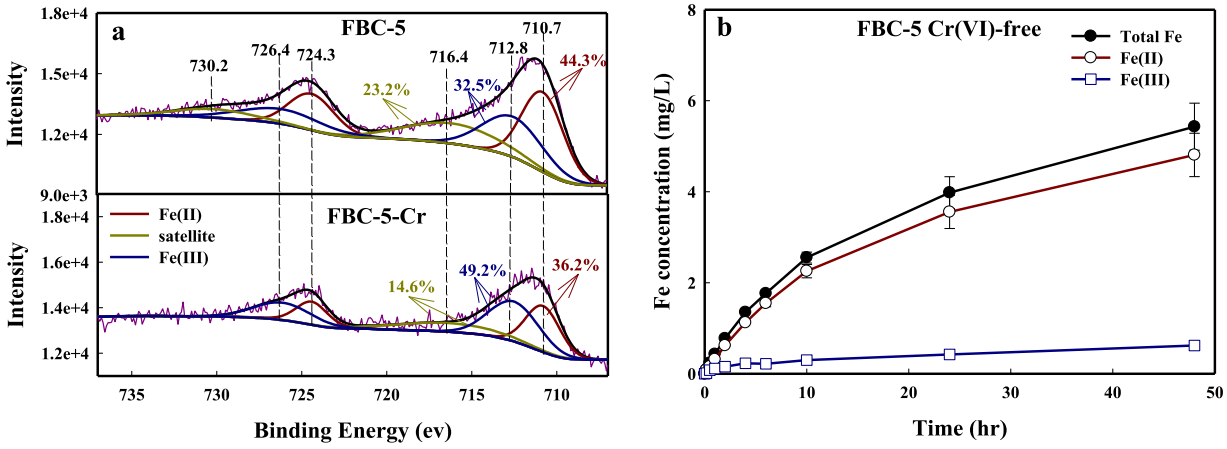

Fig. 4 – Fe 2p3/2 XPS spectra of FBC-5 before and after Cr(VI) removal (a). Fe release kinetics of FBC-5 in the absence of Cr(VI) (b).

the present study was only 1.33% within 48 hr, as reported by Chen et al. (2021), the Cr(VI) reduction efficiencies of dissolved biochar were negligible in the dark condition.

2.3. *Effect of Fe(II) on Cr(VI) reduction*

Iron oxides were successfully loaded on the biochar after $FeCl_3$ modification and could affect the reduction of Cr(VI). The presence of Fe on the surface of FBC-5 was confirmed by the EDS analysis (Appendix A Fig. S2). Iron oxides of FBCs were identified by XRD, including Fe_3O_4 and $FeCl_2$ (Appendix A Fig. S4a) (Fang et al., 2015). Before Cr(VI) removal, Fe(II) (710.7 and 724.3 eV), Fe(III) (712.8 and 726.4 eV), and satellite peaks of Fe(II) (716.4 and 730.2 eV) were observed in the Fe 2p3/2 XPS spectra of FBC-5 (Fig. 4a) (Yamashita and Hayes, 2008). After Cr(VI) removal, the Fe(II) on FBC-5 decreased from 44.3% to 36.2%, the satellite peak of Fe(II) decreased from 23.2% to 14.6%, and the Fe(III) increased from 32.5% to 49.2% (Fig. 4a), indicating that electron transfer occurred between solid Fe(II) and the adsorbed Cr(VI). However, the Fe content in FBC-1 is too low to be detected by XPS (Appendix A Fig. S6a). A previous study reported that iron oxide Fe(II) (Fe_3O_4) loaded on the magnetically modified biochar disappeared owing to Fe_3O_4 converted to γ-Fe_2O_3 after Cr(VI) reduction (Zhong et al., 2018). However, 36.2% of Fe(II) still existed on the surface of FBC-5 after Cr(VI) reduction, which was possibly due to the re-reduction of Fe(III) by the reductive substances (such as PFRs) of FBC-5 (detailed in the following section).

Besides the iron oxide Fe(II) in Fe_3O_4, the ionic Fe(II) in $FeCl_2$ also existed in FBCs (Appendix A Fig. S4a), indicating that Fe(II) could be easily released into the solution and participated in Cr(VI) reduction. Fe(II) ion is an important reductant with a low standard electrode potential of 0.77 V/SHE and can transform Cr(VI) to Cr(III) ($E^0(HCrO_4^-/Cr^{3+}) = 1.35$ V/SHE) (Buerge and Hug, 1999; Jiang et al., 2019). In the present study, Fe(II) was only detected in the control group (without Cr(VI)) of the FBC-5 system with concentration increasing from 0 to 4.81 mg/L within 48 hr (Fig. 4b and Appendix A Fig. S6b). In contrast, no Fe(II) ion was detected in the experimental group (with Cr(VI)) of the FBC-5 system, indicating that Fe(II) released by FBC-5 was immediately oxidized by Cr(VI) (Eq. (1)). However, no Fe(III) ion was detected in the experimental group of FBC-5 system. The foremost reason is that the generated Fe(III) was separated from the solution in the form of insoluble precipitates and tended to evolve into metal and/or mixed metal hydroxides, such as $Cr(OH)_3$ and $Cr_xFe_{1-x}(OH)_3$/$Cr_xFe_{1-x}OOH$ (Eqs. (2) and (3)) (Dong et al., 2017; Qiu et al., 2020). The secondary factor is that Fe(III) could be precipitated by hydrolysis when pH is larger than 3 (Eq. (4)). By increasing the dosage of FBC-5 and decreasing the initial Cr(VI) concentration and pH, Fe(II) was still undetectable until Cr(VI) was completely removed from the solution (Appendix A Fig. S5), consistent with the result of the previous study (Su et al., 2021). Moreover, when aqueous Fe(II) reduces Cr(VI) to Cr(III) in the absence of biochar, the stoichiometric ratio between Cr(VI) and Fe(II) is 1:3 (Xu et al., 2020b). However, the released concentration of Fe(II) with FBC-5 in this study was much lower than its reduction amount of Cr(VI), so there were other reductive substances involved in Cr(VI) transformation.

$$HCrO_4^- + 3Fe^{2+} + 7H^+ \rightarrow Cr^{3+} + 3Fe^{3+} + 4H_2O \quad (1)$$

$$(1\text{-}x)Fe^{3+} + xCr^{3+} + 3H_2O \rightarrow Cr_xFe_{1-x}(OH)_3 + 3H^+ \quad (2)$$

$$(1\text{-}x)Fe^{3+} + xCr^{3+} + 2H_2O \rightarrow Cr_xFe_{1-x}OOH + 3H^+ \quad (3)$$

$$2Fe^{3+} + 6H_2O \rightarrow 2Fe(OH)_{3(s)} + 6H^+ \quad (4)$$

2.4. *Effect of PFRs on Cr(VI) reduction*

PFRs with delocalized unpaired electrons can directly react with contaminants by single-electron transfer, and their concentrations and types mainly dominate the redox reactivity of PFRs (Zhu et al., 2020; Ruan et al., 2019). $FeCl_3$ modification effectively altered the PFRs concentration of biochar (Fig. 5a), especially for FBC-1, which increased dramatically from 0.639 × 10^{18} to 4.28 × 10^{18} spins/g. However, excessive

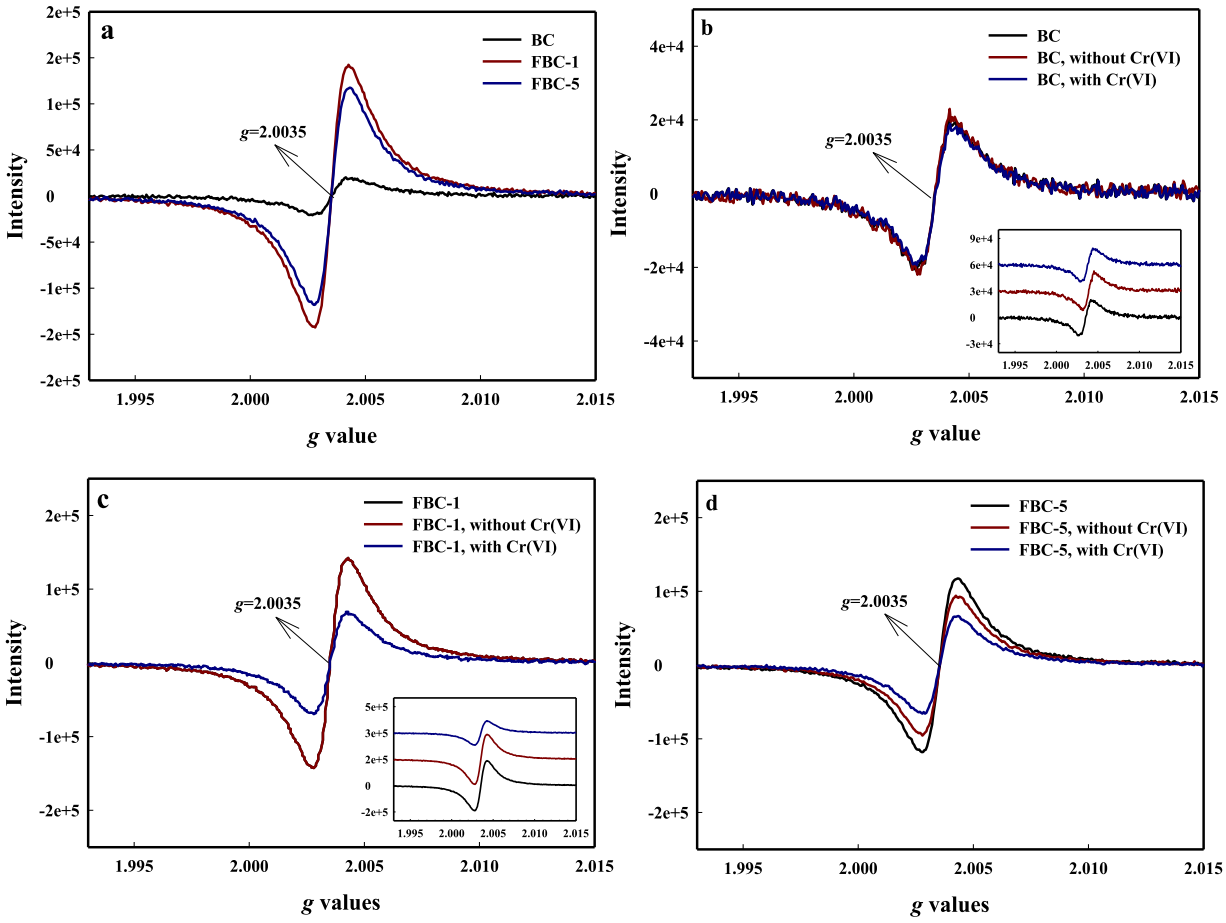

Fig. 5 – EPR signals of BC and FBCs at 500°C (a) and after Cr(VI) removal (b-d). Some EPR signals in figures b and c completely overlap, so they are displayed as a small graph.

Fe can quench PFRs, such as the PFRs concentration in FBC-5 (3.00×10^{18} spins/g) that is lower than in FBC-1. When biochar was loaded with a low concentration of Fe(III), Fe(III) can accept electrons from biochar organic matter (such as phenolic compounds) and favor the formation of PFRs (Fang et al., 2015). In contrast, when biochar loaded with a relatively high concentration of Fe(III), the excess Fe(III) would consume PFRs, since PFRs can act as an electron donor to mediate the reduction of Fe(III) (Klüpfel et al., 2014; Kappler et al., 2014). This could account for the presence of $FeCl_2$ in FBC-5 (Appendix A Fig. S4a). The corresponding spectroscopic splitting factors (*g* values) of BC and FBCs from the EPR signal were 2.0035, indicating that the carbon-centered PFRs with an adjacent oxygen atom (phenoxyl radicals) formed in biochar during the pyrolysis process and have high electron donor capacity (Li et al., 2017; Vejerano et al., 2011). In this study, $FeCl_3$ doping just changed the concentration of PFRs in the biochar but did not change the type of PFRs.

EPR analysis was performed on BC and FBCs at 48 hr of sorption kinetic. In the control groups without Cr(VI) (Fig. 5b and 5c), PFRs concentrations of BC and FBC-1 were the same as the pristine BC and FBC-1. However, the PFRs concentration of FBC-5 in the control group decreased from 3.00×10^{18} spins/g to 2.86×10^{18} spins/g. The decreased PFRs in FBC-5 may participate in the reduction of Fe(III) and inhibit the oxidation of Fe(II) (Fig. 5d). Similarly, Qin et al. (2017) reported that PFRs on the biochar surface can promote Fe(III) reduction to Fe(II) through single electron transfer. In the experimental groups, the PFRs concentrations for BC, FBC-1, and FBC-5 decreased markedly from 0.639×10^{18} to 0.595×10^{18} spins/g, 4.28×10^{18} to 2.09×10^{18} spins/g, and 2.86×10^{18} to 1.98×10^{18} spins/g, respectively, revealing that PFRs on the BC and FBCs were consumed during the removal of Cr(VI). The *g* values of the FBCs (2.0035) were close to the free-electron *g* factor (2.0023), suggesting that the PFRs have similar properties to free electrons and can directly donate electrons to reduce Cr(VI) into Cr(III) (Xu et al., 2020a; Zhao et al., 2018). In addition, previous studies reported that phenoxyl-type PFRs had a lower Mulliken charge (0.150 e) and thus had a higher electron-donating ability to reduce Cr(VI) (Zhong et al., 2018; Li et al., 2017). Moreover, the solid phase PFRs quenching experiment and solution phase competitive electron donor addition experiment all indicated the direct electron donor ability of PFRs (Fig. 6, detailed in the following section). Besides direct electron transfer, the PFRs of biochar can transfer electrons to O_2 to produce superoxide anions ($O_2^{\bullet-}$) and indirectly reduce Cr(VI) to Cr(III) (Chen et al., 2021; Zhong et al., 2018). But this indirect electron transport pathway of PFRs may not occur since no $O_2^{\bullet-}$ was observed in

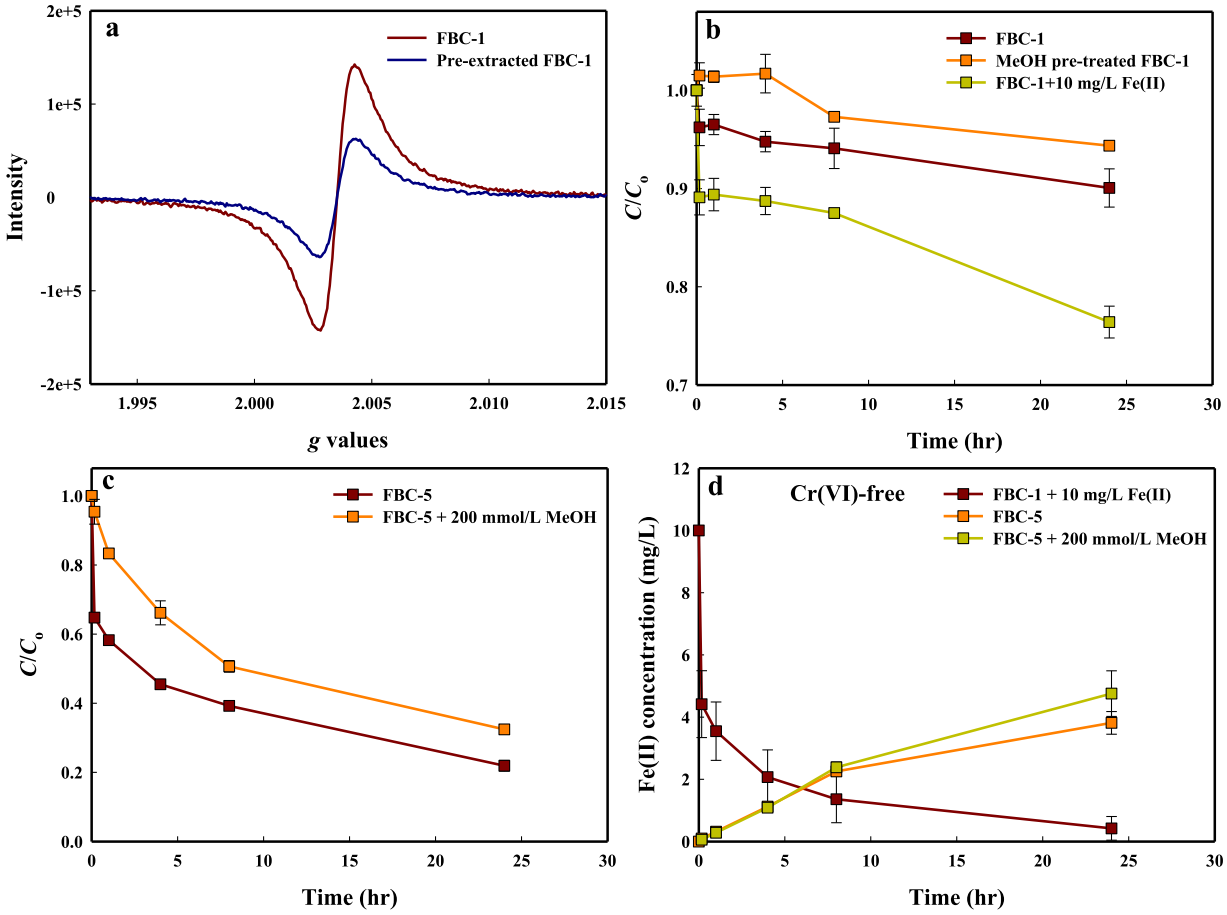

Fig. 6 – EPR signals of FBC-1 and methanol (MeOH) pre-treated FBC-1 (a). Impacts of Fe(II) reductant (b) and MeOH competitive electron (c) on Cr(VI) removal efficiency and Fe(II) concentration (d). Conditions of figures b and c: [Biochar] = 5.0 g/L, [initial Cr(VI)] = 100 mg/L, [initial pH] = 5.0 ± 0.1, [temperature] = 25 ± 1°C. Conditions of figure d: [Biochar] = 5.0 g/L, [initial Cr(VI)] = 0 mg/L, [initial pH] = 5.0 ± 0.1, [temperature] = 25 ± 1°C.

the control and experimental groups in this study (Appendix A Fig. S7). In general, the above results collectively indicated that PFRs was one key factor that dominated the transformation of Cr(VI).

Notably, the PFRs concentration of FBC-1 was higher than that of FBC-5, but the Cr(VI) reduction efficiency of FBC-1 was much lower. The higher reduction by FBC-5 may be associated with the significantly more Fe(II) (44.3% measured by XPS) than FBC-1. Therefore, Fe(II) and PFRs may be the two coupling factors that influence the reduction of Cr(VI) by biochar. To confirm the effect of PFRs and Fe(II) on the transformation of Cr(VI), PFRs quenching and an extra reductant (Fe(II)) addition experiment was conducted. Considering that Fe(III) is prone to hydrolysis at pH >3, Fe(II) was added as the reductant in this experiment. Methanol could effectively trap PFRs (Zhu et al., 2020). FBC-1 with the highest PFRs concentration was selected to conduct a methanol pre-extracted quenching experiment. By comparing with the unquenched experiment, the PFRs concentration of FBC-1 decreased significantly from 4.28×10^{18} spins/g to 1.92×10^{18} spins/g (Fig. 6a), the Cr(VI) removal efficiency of FBC-1 decreased from 9.95% to 5.63% at 24 hr (Fig. 6b), and the Cr(III) concentration decreased from 5.87 mg/L to 1.16 mg/L (Appendix A Fig. S8a). The results illustrated that the concentration of PFRs directly determines its electron donor capability and further affected the conversion efficiency of Cr(VI), consistent with Zhu et al. (2020). When 10 mg/L Fe(II) was added to FBC-1 system, a higher removed concentration of Cr(VI) (9.95 vs. 23.6 mg/L) was observed (Fig. 6b). Generally, the stoichiometric ratio between Cr(VI) and Fe(II) was 1:3 (Xu et al., 2020b). This indicated that 10 mg/L Fe(II) could theoretically reduce about 3.3 mg/L Cr(VI), much lower than the increased removal amount of Cr(VI) (13.7 mg/L). In addition, in the control group, the Fe(II) content decreased along with the reaction time, and no Fe(III) was detected in the solution, indicating that Fe(II) was adsorbed to the FBC-1 surface (Fig. 6d). Previous studies demonstrated that PFRs on biochar could act as an electron donor and accelerate electron transfer from biochar to Fe(III) ions to promote surface Fe(III)/Fe(II) cycling (Qin et al., 2017; Wang et al., 2020). Thus, the PFRs on the FBC-1 surface may accelerate Fe(III)/Fe(II) cycling and subsequently enhance Cr(VI) removal. This also contributed to a large amount of Fe(II) in the solid phase of FBC-5 after the removal of Cr(VI).

When 200 mmol/L MeOH was added to the FBC-5 system, the Cr(VI) removal efficiency decreased from 35.2% to 4.5% within 0.17 hr and decreased from 78.1% to 67.5% within 24

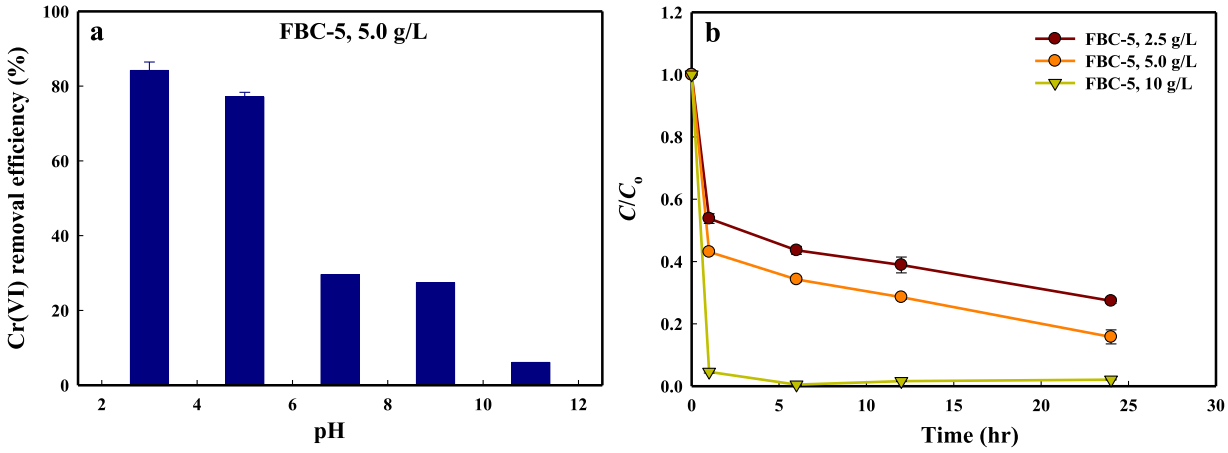

Fig. 7 – Effects of initial pH (a) and dosage (b) on Cr(VI) removal efficiency of FBC-5. Conditions of figure a: [FBC-5] = 5.0 g/L, [initial Cr(VI)] = 100 mg/L, [temperature] = 25 ± 1°C, [reaction time] = 24 hr. Conditions of figure b: [initial Cr(VI)] = 100 mg/L, [initial pH] = 3.0 ± 0.1, [temperature] = 25 ± 1°C.

hr, and the Cr(III) concentration decreased from 6.63 mg/L to 3.38 mg/L (Fig. 6c and Appendix A Fig. S8b). Whether MeOH was added or not, the Fe(II) content in the FBC-5 control group showed little change (Fig. 6d), suggesting that MeOH did not affect the release of Fe(II) from FBC-5. MeOH can act as an electron competitor to consume PFRs, thus constraining the Fe(III)/Fe(II) cycle and further inhibiting the reduction of Cr(VI). The above experiments, including the addition of a reductant (Fe(II)) and competitive electron (MeOH), indicated a significant synergistic effect of PFRs and Fe(II) on Cr(VI) reduction. PFRs on biochar surfaces can promote the Fe(III)/Fe(II) cycle through single electron transfer and accelerate the reduction of Cr(VI).

2.5. *Effect of pH and reactant dosage on Cr(VI) removal*

The removal efficiency of Cr(VI) that depends on the surface adsorption sites and reductive ability of heterogeneous materials is greatly affected by the initial solution pH and reactant dosage (Wang et al., 2020). The Cr(VI) removal efficiency for the FBC-5 system was examined at initial pH values of 3.0–11.0 and slightly decreased from 84.2% to 77.1% and then sharply decreased to 6.08% with the initial solution pH increased from 3.0 to 5.0 and 11.0, respectively (Fig. 7a). These results indicated an inescapable effect of initial solution pH on Cr(VI) removal. When the initial pH was 3.0–5.0, the FBC-5 surface was positively charged (Appendix A Fig. S1b), which allowed the electrostatic adsorption of the negatively charged Cr(VI) ion ($HCrO_4^-$) to its surface (Zhong et al., 2018). Additionally, the lower pH promotes the dissolution of Fe_3O_4 to release Fe(II) that subsequently contributes to the reduction of Cr(VI) in the aqueous phase. However, the surface charge of FBC-5 became more negative with increasing pH from 7.0 to 11.0 (Appendix A Fig. S1b). Moreover, Fe(III) ions are hydrolyzed/precipitated under alkaline conditions, which results in a high passivation surface of FBC-5 and further limits on Cr(VI) reduction. The results indicated that pH could alter the surface charge and solubility of FBC-5.

The Cr(VI) removal efficiency at different FBC-5 dosages in the range of 2.5–10 g/L was also evaluated. The Cr(VI) removal efficiency of the FBC-5 dosages at 2.5 g/L was 72.6% and reached up to 84.2% at 5 g/L and 100% at 10 g/L, respectively (Fig. 7b). Higher dosages of FBC-5 provide more adsorption sites and reductive species and promote greater dissolution of iron oxide loaded on the biochar, accelerating the removal of Cr(VI).

2.6. *Cr(VI) reduction mechanism by BC and FBCs*

In this study, reduction and immobilization were the main removal process of Cr(VI) by BC and FBCs. For BC system, the Cr(VI) anions were adsorbed on the surface of biochar through complexation with surface functional groups and were partially reduced to Cr(III) by reductive functional groups (C-O). In addition, PFRs on the surface of BC participated in the reduction of Cr(VI) by direct electron transfer. For the FBCs systems, the mechanisms of Cr(VI) removal by PFRs and Fe(II) were proposed and illustrated in Scheme 1: the electrostatic attraction between Cr(VI) anions (e.g. $HCrO_4^-$) and the positive surface charge of FBCs were responsible for the rapid removal of Cr(VI) at the initial stage of the reaction (Fig. 1 and Appendix A Fig. S1). The adsorbed Cr(VI) was further reduced to Cr(III) by the C-O group or Fe(II) on the surface of FBCs. Moreover, PFRs on the FBCs surface promoted the Fe(III)/Fe(II) cycle by transferring electrons to Fe(III), which synergistically enhanced the reduction of Cr(VI). The contribution of the PFRs to Cr(VI) reduction could be evaluated. By assuming that all the processes includ-

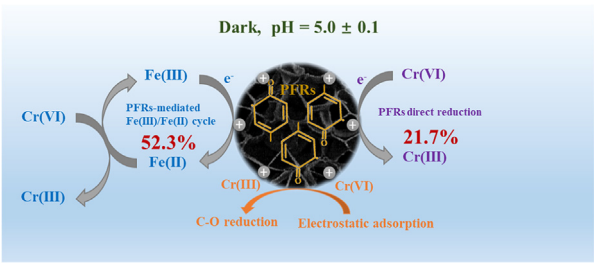

Scheme 1 – Schematic illustration for the Cr(VI) reduction pathways by FBCs.

ing dissolved Fe(II), direct PFRs reduction, and PFRs-mediated Fe(III)/Fe(II) cycle involved are independent. Take FBC-1 system as an example, we defined the difference between FBC-1 and MeOH pre-extracted FBC-1 that was used for Cr(VI) removal (9.95 vs 5.63 mg/L) as the direct PFRs reduction. In addition, when 10 mg/L Fe(II) was added to FBC-1 system and all of them that participate in the reduction of Cr(VI) can only reduce 3.3 mg/L Cr(VI), the remaining 10.4 mg/L Cr(VI) was reduced by PFRs-mediated Fe(III)/Fe(II) cycle. The total reduction amount of Cr(VI) in the FBC-1 system with Fe(II) added was calculated to be 19.9 mg/L. The direct PFRs reduction and PFRs-mediated Fe(III)/Fe(II) cycle could account for 21.7% and 52.3% for Cr(VI) reduction, respectively. The high contribution of PFRs-mediated Fe(III)/Fe(II) cycle indicated the significant synergistic effect of PFRs and Fe(II) on Cr(VI) reduction.

3. Conclusions

Iron-modified biochar was prepared with $FeCl_3$ and its environmental implications on Cr(VI) transformation were investigated. Compared with unmodified BC, $FeCl_3$ modification increased the surface charge, content of reductive oxygen-containing functional groups (C-O), and concentration of reductive phenoxyl-type PFRs. In addition, low $FeCl_3$-doping biochar (FBC-1) effectively enhanced Cr(VI) removal efficiency and Cr(VI) reduction efficiency by 1.54 and 1.88 fold due to the increased PFRs, respectively. In contrast, high $FeCl_3$-doping biochar (FBC-5) significantly promoted the Cr(VI) removal efficiency and Cr(VI) reduction efficiency which was significantly higher than the BC and FBC-1. Although FBC-5 had a lower PFRs concentration than FBC-1, the PFRs on the FBC-5 surface accelerate electron transfer from biochar to Fe(III) ions to promote Fe(III)/Fe(II) cycling that enhanced the conversion of Cr(VI) to Cr(III). Based on our work, we recommended that modification with appropriate high content of iron (5%) can significantly increase the removal of Cr(VI) from the environment. This study provides a new pathway for environmental pollutant control and remediation of oxyanion metals by iron-modified biochar.

Declaration of Competing Interest

The authors declare that they have no known competing financial interests or personal relationships that could have appeared to influence the work reported in this paper.

Acknowledgments

This work was supported by the National Key Research and Development Program of China (No. 2020YFC1808500), the National Natural Science Foundation of China (Nos. 42107046 and 41907119), the GDAS' Project of Science and Technology Development (Nos. 2022GDASZH-2022010105, and 2019GDASYL-0102002-5), the Postdoctoral Science Foundation of China (No. 2020M682634), and the Guangdong Basic and Applied Basic Research Foundation (No. 2021A1515011540).

Appendix A Supplementary data

Supplementary material associated with this article can be found, in the online version, at doi:10.1016/j.jes.2023.03.011.

References

Buerge, I.J., Hug, S.J., 1999. Influence of mineral surfaces on chromium (VI) reduction by iron (II). Environ. Sci. Technol. 33, 4285–4291.

Chacón, F.J., Sánchez-Monedero, M.A., Lezama, L., Cayuela, M.L., 2020. Enhancing biochar redox properties through feedstock selection, metal preloading and post-pyrolysis treatments. Chem. Eng. J. 395, 125100.

Chen, N., Cao, S.Y., Zhang, L., Peng, X., Wang, X.B., Ai, Z.H., et al., 2021. Structural dependent Cr(VI) adsorption and reduction of biochar: hydrochar versus pyrochar. Sci. Total Environ. 783, 147084.

Cuong, D.V., Wu, P.C., Chen, L.I., Hou, C.H., 2021. Active MnO_2/biochar composite for efficient As(III) removal: Insight into the mechanisms of redox transformation and adsorption. Water Res 188, 116495.

Dong, X.L., Ma, L.Q., Gress, J., Harris, W., Li, Y.C., 2014. Enhanced Cr(VI) reduction and As(III) oxidation in ice phase: important role of dissolved organic matter from biochar. J. Hazard. Mater. 267, 62–70.

Dong, H.R., Deng, J.M., Xie, Y.K., Zhang, C., Jiang, Z., Cheng, Y.J., et al., 2017. Stabilization of nanoscale zero-valent iron (nZVI) with modified biochar for Cr(VI) removal from aqueous solution. J. Hazard. Mater. 332, 79–86.

Fang, G.D., Liu, C., Gao, J., Dionysion, D.D., Zhou, D.M., 2015. Manipulation of persistent free radicals in biochar to activate persulfate for contaminant degradation. Environ. Sci. Technol. 49 (9), 5645–5653.

Fei, Y.H., Li, M.Z., Ye, Z.F., Guan, J.Y., Huang, Z.H., Xiao, T.F., et al., 2022. The pH-sensitive sorption governed reduction of Cr(VI) by sludge derived biochar and the accelerating effect of organic acids. J. Hazard. Mater. 423, 127205.

Fendorf, S.E., 1995. Surface reactions of chromium in soils and waters. Geoderma 67, 55–71.

Gonzalez, A.R., Ndung'u, K., Flegal, A.R., 2005. Natural occurrence of hexavalent chromium in the Aromas Red Sands Aquifer. California. Environ. Sci. Technol. 39, 5505–5511.

Han, H.W., Song, P.Z., Cai, Z.S., Dong, W.J., Khan, A., Yang, K., et al., 2022. Immobilizing chromate reductase NfoR on magnetic biochar reduced Cr(VI) in copper-containing wastewater. J. Clean. Prod. 361, 132118.

Hu, S.J., Zhang, D.N., Yang, Y., Ran, Y., Mao, J.D., Chu, W.Y., et al., 2019. Effects of the chemical structure, surface, and micropore properties of activated and oxidized black carbon on the sorption and desorption of phenanthrene. Environ. Sci. Technol. 53 (13), 7683–7693.

Jiang, B., Gong, Y.F., Gao, J.N., Sun, T., Liu, Y.J., Oturan, N., et al., 2019. The reduction of Cr(VI) to Cr(III) mediated by environmentally relevant carboxylic acids: State-of-the-art and perspectives. J. Hazard. Mater. 365, 205–226.

Kappler, A., Wuestner, M.L., Ruecker, A., Harter, J., Halama, M., Behrens, S., 2014. Biochar as an electron shuttle between bacteria and Fe(III) minerals. Environ. Sci. Technol. Lett. 1, 339–344.

Kemper, J.M., Ammar, E., Mitch, W.A., 2008. Abiotic degradation of hexahydro-1,3,5-trinitro-1,3,5-triazine in the presence of hydrogen sulfide and black carbon. Environ. Sci. Technol. 42 (6), 2118–2123.

Klüpfel, L., Keiluweit, M., Kleber, M., Sander, M., 2014. Redox properties of plant biomass-derived black carbon (biochar). Environ. Sci. Technol. 48, 5601–5611.
Kyzas, G.Z., Lazaridis, N.K., Mitropoulos, A.C., 2012. Removal of dyes from aqueous solutions with untreated coffee residues as potential low-cost adsorbents: Equilibrium, reuse and thermodynamic approach. Chem. Eng. J. 189, 148–159.
Lehmann, J., Rillig, M.C., Thies, J., Masiello, C.A., Hockaday, W.C., Crowley, D., 2011. Biochar effects on soil biota – A review. Soil Biol. Biochem. 43 (9), 1812–1836.
Li, J.Y., Wang, Y.R., Song, J., Gao, Q., Zhang, J., Zhang, J.Y., et al., 2017. Theoretical and experimental evidence for the carboneoxygen group enhancement of NO reduction. Environ. Sci. Technol. 51, 14209–14216.
Liang, L.P., Guan, X.H., Shi, Z., Li, J.L., Wu, Y.N., Tratnyek, P.G., 2014. Coupled effects of aging and weak magnetic fields on sequestration of selenite by zero-valent iron. Environ. Sci. Technol. 48, 6326–6334.
Liang, S., Zhu, L.Y., Hua, J., Duan, W.J, Yang, P.T., Wang, S.L., et al., 2020. Fe^{2+}/HClO reaction products produces $Fe^{IV}O^{2+}$: An enhanced advanced oxidation process. Environ. Sci. Technol. 54, 6406–6414.
Lima, H.H.C., Maniezzo, R.S., Kuffer, V.L., Guilherme, M.R., Moises, M.P., Arroyo, P.A., et al., 2018. Hydrochars based on cigarette butts as a recycled material for the adsorption of pollutants. J. Environ. Chem. Eng. 6 (06), 7054–7061.
Liu, J., Jiang, J., Meng, Y., Aihemaiti, A., Xu, Y., Xiang, H., et al., 2020. Preparation, environmental application and prospect of biochar-supported metal nanoparticles: A review. J. Hazard. Mater. 388, 122026.
Mandal, S., Pu, S.Y., Adhikari, S., Ma, H., Kim, D.H., Bai, Y.C., et al., 2021. Progress and future prospects in biochar composites: Application and reflection in the soil environment. Crit. Rev. Environ. Sci. Technol. 51, 219–271.
Mian, M.M., Liu, G.J., Yousaf, B., Fu, B., Ullah, H., Ali, M.U., et al., 2018. Simultaneous functionalization and magnetization of biochar via NH_3 ambiance pyrolysis for efficient removal of Cr(VI). Chemosphere 208, 712–721.
Park, D., Yun, Y.S., Park, J.M., 2004. Reduction of hexavalent chromium with the brown seaweed Ecklonia biomass. Environ. Sci. Technol. 38 (18), 4860–4864.
Pechova, A., Pavlata, L., 2007. Chromium as an essential nutrient: a review. Vet. Med. 52, 1–18.
Qin, Y.X., Zhang, L.Z., An, T.C., 2017. Hydrothermal carbon-mediated Fenton-like reactionmechanism in the degradation of Alachlor: direct electron transfer from hydrothermal carbon to Fe(III). ACS Appl. Mater. Interfaces. 9, 17115–17124.
Qiu, Y., Zhang, Q., Gao, B., Li, M., Fan, Z.X., Sang, W.J., et al., 2020. Removal mechanisms of Cr(VI) and Cr(III) by biochar supported nanosized zero-valent iron: Synergy of adsorption, reduction and transformation. Environ. Pollut. 265, 115018.
Rajput, S., Pittman, Jr C.U., Mohan, D., 2016. Magnetic magnetite (Fe_3O_4) nanoparticle synthesis and applications for lead (Pb^{2+}) and chromium (Cr^{6+}) removal from water. J. Colloid Interface Sci. 468, 334–346.
Ruan, X.X., Sun, Y.Q., Du, W.M., Tang, Y.Y., Liu, Q., Zhang, Z.Y., et al., 2019. Formation, characteristics, and applications of environmentally persistent free radicals in biochars: a review. Bioresour Technol 281, 457–468.
Shen, Y.W., Yu, Y.M., Zhang, Y., Urgun-Demirtas, M., Yuan, H.P., Zhu, N.W., et al., 2021. Role of redox-active biochar with distinctive electrochemical properties to promote methane production in anaerobic digestion of waste activated sludge. J. Clean. Prod. 278, 123212.
Shi, Y.F., Dai, Y.C., Liu, Z.W., Nie, X.F., Zhao, S., Zhang, C., et al., 2020. Light-induced variation in environmentally persistent free radicals and the generation of reactive radical species in humic substances. Front. Environ. Sci. Eng. 14 (6), 106.
Su, C.L., Wang, S., Zhou, Z.Y., Wang, H.J., Xie, X.J., Yang, Y.Y., et al., 2021. Chemical processes of Cr(VI) removal by Fe-modified biochar under aerobic and anaerobic conditions and mechanism characterization under aerobic conditions using synchrotron-related techniques. Sci. Total Environ. 768, 144604.
Tamura, H., Goto, K., Yotsuyanagi, T., Nagayama, M., 1974. Spectrophotometric determination of iron(II) with 1, 10-phenanthroline in the presence of large amounts of iron(III). Talanta 21, 314–318.
Tang, Z., Kong, Y.F., Zhao, S., Jia, H.Z., Vione, D., Kang, Y.M., et al., 2021. Enhancement of Cr(VI) decontamination by irradiated sludge biochar in neutral conditions: Evidence of a possible role of persistent free radicals. Sep. Purif. Technol 277, 119414.
Vejerano, E., Lomnicki, S., Dellinger, B., 2011. Formation and stabilization of combustion-generated environmentally persistent free radicals on an $Fe(III)_2O_3$/silica surface. Environ. Sci. Technol. 45, 589–594.
Vithanage, M., Herath, I., Joseph, S., Bundschuh, J., Bolan, N., Ok, Y.S., et al., 2017. Interaction of arsenic with biochar in soil and water: A critical review. Carbon 113, 219–230.
Wang, X.D., Xu, J., Liu, J., Liu, J., Xia, F., Wang, C.C., et al., 2020. Mechanism of Cr(VI) removal by magnetic greigite/biochar composites. Sci. Total Environ. 700, 134414.
Wu, F.C., Tseng, R.L., Juang, R.S., 2009. Characteristics of Elovich equation used for the analysis of adsorption kinetics in dye-chitosan systems. Chem. Eng. J. 150, 366–373.
Xu, J., Dai, Y.C., Shi, Y.F., Zhao, S., Tian, H.X., Zhu, K.C., et al., 2020a. Mechanism of Cr(VI) reduction by humin: Role of environmentally persistent free radicals and reactive oxygen species. Sci. Total Environ. 725, 138413.
Xu, X.Y., Huang, H., Zhang, Y., Xu, Z.B., Cao, X.D., 2019. Biochar as both electron donor and electron shuttle for the reduction transformation of Cr(VI) during its sorption. Environ. Pollut. 244, 423–430.
Xu, W.Q., Pignatello, J.J., Mitch, W.A., 2013. Role of black carbon electrical conductivity in mediating Hexahydro-1,3,5-trinitro-1,3,5-triazine (RDX) transformation on carbon surfaces by sulfides. Environ. Sci. Technol. 47 (13), 7129–7136.
Xu, Z.B., Xu, X.Y., Tsang, D.C.W., Yang, F., Zhao, L., Qiu, H., et al., 2020b. Participation of soil active components in the reduction of Cr(VI) by biochar: Differing effects of iron mineral alone and its combination with organic acid. J. Hazard. Mater. 384, 121455.
Yamashita, T., Hayes, P., 2008. Analysis of XPS spectra of Fe^{2+} and Fe^{3+} ions in oxide materials. Appl. Surf. Sci. 254, 2441–2449.
Yang, J., Pan, B., Li, H., Liao, S.H., Zhang, D., Wu, M., et al., 2016a. Degradation of p-nitrophenol on biochars: role of persistent free radicals. Environ. Sci. Technol. 50, 694–700.
Yang, J.P., Zhao, Y.C., Ma, S.M., Zhu, B.B., Zhang, J.Y., Zheng, C.G., 2016b. Mercury removal by magnetic biochar derived from simultaneous activation and magnetization of sawdust. Environ. Sci. Technol. 50, 12040–12047.
Yi, K.X., Lei, M., Peng, L., Chen, A.W., Luo, S., 2021. Sunlight-driven degradation of diethyl phthalate via magnetically modified biochar catalysts in water: Internal electron transfer mechanism. Chemosphere 269, 129366.
Zhang, K.K., Khan, A., Sun, P., Zhang, Y., Taraqqi-A-Kamal, A., Zhang, Y.R., 2020. Simultaneous reduction of Cr(VI) and oxidization of organic pollutants by rice husk derived biochar and the interactive influences of coexisting Cr(VI). Sci. Total Environ. 706, 135763.
Zhang, Y., Yang, R.X., Si, X.H., Duan, X.W., Quan, X., 2019. The adverse effect of biochar to aquatic algae- the role of free radicals. Environ. Pollut. 248, 429–437.
Zhao, N., Yin, Z., Liu, F., Zhang, M.Y., Lv, Y.Z., Hao, Z.P., et al., 2018. Environmentally persistent free radicals mediated removal of

Cr(VI) from highly saline water by corn straw biochars. Bioresour Technol 260, 294–301.
Zhong, D.L., Zhang, Y.R., Wang, L.L., Chen, J., Jiang, Y., Tsang, D.C.W., et al., 2018. Mechanistic insights into adsorption and reduction of hexavalent chromium from water using magnetic biochar composite: key roles of Fe_3O_4 and persistent free radicals. Environ. Pollut. 243, 1302–1309.
Zhou, L., Chi, T.Y., Zhou, Y.Y., Lv, J.D., Chen, H., Sun, S.Q., et al., 2022. Efficient removal of hexavalent chromium through adsorption-reduction-adsorption pathway by iron-clay biochar composite prepared from Populus nigra. Separ. Purif. Technol. 285, 120386.
Zhu, S.S., Huang, X.C., Yang, X.B., Peng, P., Li, Z.P., Jin, C., 2020. Enhanced transformation of Cr(VI) by heterocyclic–N within nitrogen-doped biochar: Impact of surface modulatory persistent free radicals (PFRs). Environ. Sci. Technol. 54, 8123–8132.